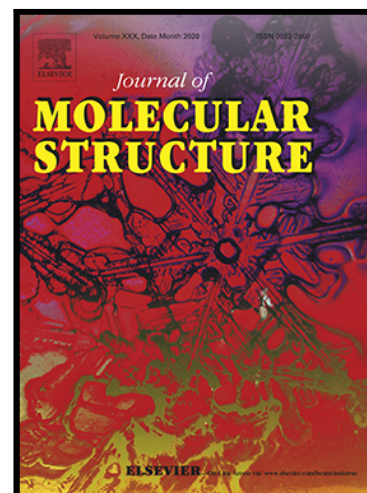


## Journal Pre-proof

Synthesis, structure, third-order nonlinear optical properties and Hirshfeld surface analysis of tetrakis(azepanium) hexachlorostannate(IV) dichloride and tetrakis(azepanium) hexabromostannate(IV) dibromide

M. Manonmani , C. Balakrishnan , M. Dhanalakshmi ,  
S. Rafi Ahamed , G. Vinitha , R.M. Sockalingam

PII: S0022-2860(20)31830-5  
DOI: <https://doi.org/10.1016/j.molstruc.2020.129515>  
Reference: MOLSTR 129515



To appear in: *Journal of Molecular Structure*

Received date: 5 June 2020  
Revised date: 21 October 2020  
Accepted date: 24 October 2020

Please cite this article as: M. Manonmani , C. Balakrishnan , M. Dhanalakshmi , S. Rafi Ahamed , G. Vinitha , R.M. Sockalingam , Synthesis, structure, third-order nonlinear optical properties and Hirshfeld surface analysis of tetrakis(azepanium) hexachlorostannate(IV) dichloride and tetrakis(azepanium) hexabromostannate(IV) dibromide, *Journal of Molecular Structure* (2020), doi: <https://doi.org/10.1016/j.molstruc.2020.129515>

This is a PDF file of an article that has undergone enhancements after acceptance, such as the addition of a cover page and metadata, and formatting for readability, but it is not yet the definitive version of record. This version will undergo additional copyediting, typesetting and review before it is published in its final form, but we are providing this version to give early visibility of the article. Please note that, during the production process, errors may be discovered which could affect the content, and all legal disclaimers that apply to the journal pertain.

© 2020 Published by Elsevier B.V.

## Highlights

- The compounds (1) and (2) are isostructural with small variations in lattice parameters.
- The band gap energies of the hybrids can be easily tuned by altering the halide ion.
- Both the hybrids possess a significant third-order nonlinear response.
- Intermolecular interactions are analyzed and quantified by 2D fingerprint plots *via* Hirshfeld surface analysis.

# Synthesis, structure, third-order nonlinear optical properties and Hirshfeld surface analysis of tetrakis(azepanium) hexachlorostannate(IV) dichloride and tetrakis(azepanium) hexabromostannate(IV) dibromide

M. Manonmani<sup>a</sup>, C. Balakrishnan<sup>a</sup>, M. Dhanalakshmi<sup>a</sup>, S. Rafi Ahamed<sup>b</sup>, G. Vinitha<sup>c</sup>,  
RM. Sockalingam<sup>a\*</sup>

<sup>a</sup> Crystal Growth Lab, Department of Chemistry, Annamalai University, Annamalaiagar, Tamil Nadu, India

<sup>b</sup> Department of Physics, Academy of Maritime Education and Training, deemed to be University, Chennai, Tamil Nadu

<sup>c</sup> Division of Physics, School of Advanced Science, VIT Chennai, Chennai, Tamil Nadu, India

## Abstract

The new organic-inorganic hybrids of tetrakis(azepanium) hexachlorostannate(IV) dichloride (**1**) and tetrakis(azepanium) hexabromostannate(IV) dibromide (**2**) crystals have been grown after slow evaporation of the solvent and characterized through single-crystal X-ray diffraction analysis. The characteristic functional groups present in the compounds are confirmed by FT-IR analysis. The direct band gap values for the compounds are estimated by the application of Kubelka-Munk function. Photoluminescence studies exhibit fluorescent emission of both the compounds in the solid-state at room temperature. TG/DTA analysis reveals the thermal pattern of the compounds. Bond valence sum (BVS) calculation confirmed the formal oxidation state of tin to be +4. Z-scan studies very much reveal that both the compounds exhibit significant third-order nonlinear optical response. Investigation of the intermolecular interactions and crystal packing using Hirshfeld surface analysis, derived by single-crystal XRD data, reveals the close contacts associated with strong interactions.

**Keywords:** Organic-inorganic hybrids; Hirshfeld surface; Z-scan studies; Band gap; Thermal pattern

## 1. Introduction

Hybrid materials are being used to systems such as metal-organic frameworks, highly ordered polymers, sol-gel compounds and macro-structured inorganic particles in the organic matrix [1]. Perovskites belong to a class of inorganic crystals with general chemical formula  $ABX_3$  composition can be constructed with various metal cations (A and B) and anions (X). In such a perovskite structure, the inorganic cations A and B are coordinated by 12 (cuboctahedral) and 6 (octahedral) anions X, respectively. The discovery is credited to Gustav Rose following his report on the oxide perovskite calcium titanate ( $CaTiO_3$ ) in 1839 [2]. Any material that adopts the same crystal structure as isostructural to  $CaTiO_3$ , namely,  $ABX_3$  structure [3], where 'A' site is occupied by an organic ammonium cation and the 'B' site by metal ion such as  $Sn^{2+}$ ,  $Pb^{2+}$ ,  $Ge^{2+}$ , etc., while the X site is occupied by a halide anion  $F^-$ ,  $Cl^-$ ,  $Br^-$  and  $I^-$  is a hybrid perovskite [4,5]. Very recently, organic-inorganic hybrid perovskites have attracted considerable attraction in a broad variety of materials, including data storage [6], ferroelectrics [7], superconductors [8], light-emitting devices [9], ionic conductors [10], solar cells [11] and nonlinear optical (NLO) materials [12].

NLO effects are extensively leveraged in optoelectronic fields such as saturable absorbers, switches and harmonic generators. In remarkable, third-order nonlinear materials have been designed and evolved to be applicable in a class of applications [13]. The exploration for new materials that illustrate large nonlinear optical properties remains strongly motivated both by the potential applications as well as the basic knowledge of photophysics that can be derived from correlations in chemical structure and nonlinear signals. General strategies for improving the third-order nonlinear susceptibility are manipulate conjugated organic molecules with highly delocalized electrons and/or push-pull nature [14], semiconductor-doped glasses with resonant enhancement [15] and metal halide perovskite films [16].

The crystal structures of bis(organic ammonium cations) with hexahalostannate(IV) [17-29] and tetrakis(organic ammonium cations) with hexachloridostannate(IV) dichlorides

[30-33] have been described. Here, we report the investigation of structural characterization, optical and third-order nonlinear optical responses of tetrakis(azepanium) hexachlorostannate(IV) dichloride (**1**), and tetrakis(azepanium) hexabromostannate(IV) dibromide (**2**) hybrid perovskites. Molecular interactions are quantified by fingerprint plots derived from Hirshfeld surfaces.

## 2. Experimental

### 2.1 Synthesis and crystal growth

#### Preparation of tetrakis(azepanium) hexachlorostannate(IV) dichloride (**1**)

Azepane (4 mM) and hydrochloric acid (3 mL) in ether were mixed at room temperature to obtain azepanium chloride precursor solution. Tin(IV) chloride was prepared by dissolving tin shots (0.118 g, 1 mM) in 5mL hydrochloric acid at room temperature (6 h). To the freshly prepared ethanolic solution of azepanium chloride precursor solution, tin(IV) chloride was added with constant stirring (Scheme 1). Colourless crystals were formed from the solution after 14-16 d. Photograph of as-grown crystals picturized in Fig. 1.

#### Preparation of tetrakis(azepanium) hexabromostannate(IV) dibromide (**2**)

Azepane (4 mM) and hydrobromic acid (3 mL) in ether were mixed at room temperature to obtain azepanium bromide precursor solution. Tin(IV) bromide was prepared by dissolving tin shots (0.118 g, 1 mM) in 5mL hydrobromic acid at room temperature (6 h). To the freshly prepared ethanolic solution of azepanium bromide precursor solution, tin(IV) bromide was added with constant stirring (Scheme 2). Crystals of the compound (**2**) suitable for X-ray analysis were grown from the saturated ethanolic solution after 14-16 d. Photograph of as-grown crystals picturized in Fig. 1.

)

## 2.2. Characterization techniques

FT-IR spectra were recorded using Shimadzu IR Affinity-1 FT-IR spectrophotometer as KBr discs. A Bruker AXS kappa apex3 CMOS X-ray diffractometer was used for single crystal XRD studies. Data were collected on a diffraction system which employs graphite monochromated MoK $\alpha$  radiation ( $\lambda = 0.71073 \text{ \AA}$ ). The structures were solved and refined by full-matrix least squares on  $F^2$  with WinGX software package utilizing SHELXT-2014/7 and shelx SHELXL version number 2014/7 and 2018/3. The UV– Diffuse Reflectance Spectra was recorded using Shimadzu UV2600 UV-Vis spectrophotometer. Photoluminescence spectrum was recorded by HJY:Fluorolig F3-111 Fluorescence spectrometer. In the Z-scan experiment, the samples were excited by continuous wave (CW) (532 nm, 50 mW) and ultrafast (800 nm, 150 fs) lasers. In CW excitation Gaussian profile from diode pumped Nd:YAG laser beam was focused on a 1 mm cuvette by the lens of focal length 3.5 cm to produce a beam waist ( $\omega_0$ ) of 15.35 mm. Thermogravimetric (TG) and differential thermal analysis (DTA) were carried out using a NETZSCH STA 449 F3 thermal analyzer using nitrogen atmosphere.

## 3. Results and discussion

### 3.1 FT-IR

The vibrational spectra of (1) and (2) are represented in Fig. S1. The bands perceived at 3424 and 3436  $\text{cm}^{-1}$  for compound (1) and (2) respectively, which corresponds to the asymmetric stretching vibrations of  $\text{NH}_2$  group. The sharp peak observed at 3155 and 3150  $\text{cm}^{-1}$  corresponds to the symmetric stretching vibrations of  $\text{NH}_2$  group for compound (1) and (2) respectively. The NH bending vibrations are perceived at 1575 and 1580  $\text{cm}^{-1}$ . The C-H stretching vibrations observed at 2935 and 2940  $\text{cm}^{-1}$ . The bands at 1350 and 1370  $\text{cm}^{-1}$  are due to the stretching modes of C–N moiety [34]. The rocking vibrations of the  $\text{CH}_2$  are observed at 880 and 878  $\text{cm}^{-1}$  for compounds (1) and (2) respectively.

### 3.2. Single-crystal X-ray structure analysis

Single crystals of tetrakis(azepanium) hexachlorostannate(IV) dichloride (**1**) and tetrakis(azepanium) hexabromostannate(IV) dibromide (**2**) suitable for X-ray analysis were collected by slow evaporation of ethanolic solutions of the reaction mixture at room temperature. Crystal data, data collection refinement parameters and the results of the analyses of compounds are exhibited in Table 1. Bond lengths, bond angles and dihedral angles are listed in Tables S1-S3. Both the compounds crystallize in the monoclinic system, with a centrosymmetric space group  $C2/m$ .

The Oak Ridge Thermal-Ellipsoid Plot (ORTEP) and molecular packing diagram of (**1**) are exhibited in Fig. 2. The compound (**1**) consists of four azepanium cations, two chloride anions and one independent octahedral  $[\text{SnCl}_6]^{2-}$  anion. The crystal structure consists of alternating organic and inorganic layers extending parallel arrangement is demonstrated in Fig. 3a. Sn–Cl bond distances range from 2.4192(9) – 2.4561(3) Å and Cl–Sn–Cl bond angles vary from 89.24(5) - 90.76(5)°. The compound shows extensive hydrogen-bonded interactions. The Sn atom is six-coordinated and forms a quasi-regular octahedral arrangement [35]. The octahedral environmental parameters of compound (**1**) is listed in Table 2. The effective coordination number is 5.9896 and bond length distortion index is 0.00674. The bond distances are similar to those found in other octahedral Sn(IV) compounds [33]. The crystal packing in (**1**) is controlled by the classical hydrogen bond, in extension to coulombic forces. In this system, azepanium cations interact with chloride anions and  $[\text{SnCl}_6]^{2-}$  octahedra *via* N–H...Cl and C–H...Cl hydrogen bonds. The inter- and intramolecular hydrogen bonds with hexachlorostannate(IV) and azepane are listed in Table 3a. Fig. 3b shows the N(1A) atom involves three-centre hydrogen bonding with three Cl atoms N(1A<sup>c</sup>)...Cl(1), N(1A<sup>c</sup>)...Cl(2)#2 and N(1A<sup>c</sup>)...Cl(1)#1 with the corresponding distances are 3.432(19) Å, 3.364(3) Å and 3.432(19) Å respectively.

The ORTEP and molecular packing diagram of (2) are exposed in Fig. 2. The compound (2) also consists of four azepanium cations, two bromide anions and one independent octahedral  $[\text{SnBr}_6]^{2-}$  anion. The crystal structure consists of alternating organic and inorganic layers extending parallel arrangement and is demonstrated in Fig. 4a. Sn–Br bond distances range from 2.5868(9) – 2.6288(13) Å and Br–Sn–Br bond angles vary from 89.39(4)-90.61(4)°. The compound shows extensive hydrogen-bonded interactions. The Sn atom is six-coordinated and forms a quasi-regular octahedral arrangement. The octahedral environmental parameters of compound (2) is listed in Table 2. The effective coordination number is 5.9882 with bond length distortion index 0.00718 and bond angle variance 0.3827° (Table 2). In this compound, azepanium cations interact with bromide anions and  $[\text{SnBr}_6]^{2-}$  octahedra *via* N–H...Br and C–H...Br hydrogen bonds. The inter- and intramolecular hydrogen bonds with hexabromostannate(IV) and azepane are listed in Table 3b. Atoms C(4), N(1) and N(2) participate in the formation of strong/weak inter- and intramolecular hydrogen bonds with Br atoms of  $[\text{SnBr}_6]^{2-}$  octahedron. Fig. 4b shows the N(1) involves three-centre hydrogen bonding with three Br atoms N(1)-H(1B<sup>a</sup>)...Br(1), N(1)-H(1B<sup>b</sup>)...Br(2) and N(1)-H(1B<sup>c</sup>)...Br(1) with the corresponding distances are 3.569 Å, 3.525 Å and 3.569 Å respectively (Table 3b). Compounds (1) and (2) are isostructural with small variations in lattice parameters. Various geometries associated with molecules have been described as ‘slightly distorted’ or severely distorted’ polyhedron. The extent of distortion of a particular molecular structure from an ideal polyhedron can be assessed by symmetry measures. Table 2 listed values indicate the fact that both the compounds are of distorted octahedral geometry.

### 3.3. Bond valence sum analysis

Bond valence sum (BVS) analysis is used to determine the valence of the central atom from the experimentally derived bond distances [36]. BVS estimations are carried out based on the bond distances obtained from the single-crystal X-ray structural analysis. Hence, BVS

studies indirectly prove the correctness of the crystal structures determined [37]. The method depends on the  $R_{ij}$  value for an  $i$ - $j$  bond which is primarily ionic [38,39]. In a compound, the oxidation state of a central atom 'i' bonded to 'j' match up to the bond valence,  $V$  and the total valence of the central atom is its oxidation state,

$$V = \sum v_{ij} = \exp[(R_o - R_{ij})/b]$$

where  $R_o$  is used as reported for a large number of ionic compounds [40] and  $R_{ij}$  is the experimentally determined bond distance. The constant  $b$  can be assumed to be 0.37 [41]. Bond valence sums of (1) and (2) are 3.95 and 3.93 respectively (Table 4), which proved the formal oxidation state of tin as 4+ unequivocally.

### 3.4. Hirshfeld surface analysis

Hirshfeld surface analysis and fingerprint plots were generated from the crystal data were carried out with the TONTO incorporated CrystalExplorer 3.1 program. A three-dimensional view of the molecular Hirshfeld surfaces [42,43] of compounds (1) and (2) are revealed in Fig. 5 shows surfaces that have been mapped over  $d_{norm}$ ,  $d_e$ ,  $d_i$  and shape index. Distances from the Hirshfeld surface to the nearest nucleus inside the surface ( $d_i$ ) and outside the surface ( $d_e$ ) were the first functions of distance explored for mapping on the surfaces. The red colour circular spots indicated as close contacts, through green to blue colour indicates long contacts and the normalized contact distance, well-defined in terms of  $d_e$ ,  $d_i$  and the van der Waals radii of the atoms. Shape index is defined as the local shape topography of the 3D surface.

The fingerprint plots [44] of (1) and (2) have spread this 2D graph as a griddle of coloured areas, over the range 0.4–3.0 Å in each of  $d_i$  and  $d_e$ . Bonding interactions are quantified for the compounds (1) and (2) are, (1): H...Cl (14.5%), Cl...H (18.3%) and H...H (67.2%). (2): H...Br (16.0%), Br...H (21.5%) and H...H (62.5%) shown in 2D fingerprint plot

(Fig. 6). The Cl...H/Br...H interactions are characterized by a spike in the bottom area whereas the H...Cl/H...Br interactions are indicated by a spike in the upper region in the fingerprint plot. The H...H interactions are marked in the middle spike of fingerprint plot. Leading interactions hold more space in the fingerprint region.

### 3.5. Diffuse reflectance spectroscopy

Diffuse reflectance spectra of (1) and (2) are shown in Fig. 7. The reflectance increased above 270 nm for (1) and 400 nm for (2). The absorption below 450 nm is of organic origin in the hybrids. The band gap was determined to be 4.23 eV and 2.98 eV for (1) and (2) respectively, using a plot of  $(F(R)h\nu)^2$  versus  $(h\nu)$  as shown in inset Fig. 7. The bromo hybrids show a lower band gap compared to chloro hybrids because of the orbital contribution to the top of the valance band [45]. Therefore, the band gaps associated with these hybrids can be easily tuned by altering the halide ion.

### 3.6. Photoluminescence spectral studies

On excitation of (1) and (2) with 277 nm and 404 nm radiations respectively, the compounds exhibited emission bands as shown in Fig. 8. The maxima appeared at 402 nm for (1) and 519 nm for (2). Relatively low full-width half-maximum associated with (2) indicates better quality of epilayer present in this compound than in (1). Besides, the proximity of emission maxima of the compounds (1) (402 nm) as well as (2) (519) shows the identical nature of the photoluminescence process responsible for the emission [46].

### 3.7. Z-scan studies

The nonlinear absorption ( $\beta$ ), nonlinear refractive index ( $n_2$ ), and third-order nonlinear susceptibility ( $\chi^{(3)}$ ) were defined by standard equations [47,48]. The NLO properties of the hybrids (1) and (2) were experimented by the Z-scan technique. Here the open and closed

aperture Z- scan curves are used for  $\beta$  and  $n_2$  measurements and this method has been broadly accepted by NLO society due to their high sensitivity and simplicity. The maximum energy density of the beam is at the focus, which is being symmetrically minimized both sides for the positive and negative values of  $z$ , this leads to the difference in laser intensity at different  $z$  positions. The transmittance intensity variations corresponding to the  $z$  values, the closed and open aperture  $z$ -scan curve can be represented. The recorded normalized transmittance for two compounds is revealed in Fig. 9.

The peak followed by a valley normalized transmittance curve obtained under the closed aperture configuration shows the characteristic self-defocusing behaviour [49,50]. The positive nonlinear absorption has been seen in all the compounds due to strong reverse saturable absorption in these materials. Third-order NLO parameters are list out in Table 5. The  $\chi^{(3)}$  values of common materials lie in the range  $10^{-12}$  to  $10^{-5}$  esu [51-55] and a comparison (Table 6) reveals that (1) and (2) possess a significant third-order nonlinear response and hence promising NLO candidate. Largest value of  $\chi^{(3)}$  and hence significantly perceived nonlinearity could be associated with intra- and intermolecular hydrogen bonds.

### 3.8. Thermal analysis

Thermogravimetric analysis (TGA) was carried out under a nitrogen atmosphere at a heating rate of  $20 \text{ K min}^{-1}$  in the temperature range of  $35\text{--}1100^\circ\text{C}$ . Thermal behaviour of (1) and (2) are exposed in Fig. 10 and the data are listed in Table 7. Compound (1) is stable up to  $238^\circ\text{C}$ . The first weight loss of 67.3% (calcd.: 67.6%) in the range of  $240\text{--}397^\circ\text{C}$ , due to the loss of four molecules of azepanium chloride. The second weight loss is due to the loss of two molecules of chlorine in the temperature range:  $398\text{--}498^\circ\text{C}$ . The final residue containing tin metal evaporated slowly above  $499^\circ\text{C}$ .

In compound (2), the first weight loss of 61.9% (calcd.: 62.2%) in the range of 245–402°C, corresponds to the loss of four molecules of azepanium bromide. The second weight loss is due to the loss of two molecules of bromine in the temperature range: 403-513°C. The final residue containing tin metal evaporated slowly above 514°C. In both the compounds, all the three processes are exothermic nature as is evident from the differential thermal analysis (DTA) curves (Fig. 10). TG–DTA curves confirmed the suggested formulae of the compound.

#### 4. Conclusions

Organic-inorganic hybrids such as tetrakis(azepanium) hexachlorostannate(IV) dichloride (1) and tetrakis(azepanium) hexabromostannate(IV) dibromide (2) have been synthesized and characterized by single-crystal X-ray diffraction techniques. IR spectral analysis of the compounds shows that different vibrational bands of the organic moiety show very little change on hybrid formation with tin. Diffuse reflectance spectral analysis showed the band gap of the chloride hybrids to be larger than the bromide analogue. Therefore, by changing the halide ion it is possible to tune the band gap of the hybrid material. Single crystal X-ray structural analysis showed the octahedral nature of the hexahalo dianions. Both tetrakis(azepanium) hexachlorostannate(IV) dichloride (1) and tetrakis(azepanium) hexabromostannate(IV) dibromide (2) crystallize in monoclinic crystal system and are isostructural with the space group  $C2/m$ . Azepanium cations capped the central hexahalo anion in the unit cell. The  $\text{SnX}_6^{2-}$  ions indicated their distorted octahedral geometry. BVS analysis established the formal oxidation state of tin as 4+.

### CRedit author statement

M. Manonmani: Methodology, Investigation and Formal analysis, C. Balakrishnan: Writing – original draft, M. Dhanalakshmi: Software and Formal analysis, S. Rafi Ahamed: Formal

analysis, G. Vinitha: Formal analysis, RM. Sockalingam: Conceptualization, Supervision, Writing- Reviewing and Editing.

#### **Declaration of competing interest**

The authors declare that they have no known competing financial interests or personal relationships that could have appeared to influence the work reported in this paper.

#### **Acknowledgements**

The authors thank DST PURSE Phase-II, Annamalai University and also thank SAIF, IIT Madras, Chennai, for providing single-crystal XRD facility.

#### **References**

- [1] B. Folch, J. Larionova, Y. Guari, L. Datas, C. Guerin, A coordination polymer precursor approach to the synthesis of NiFe bimetallic nanoparticles within hybrid mesoporous silica, *J. Mater. Chem.*, 16 (2006) 4435-4442.
- [2] G. Rose, *De novis quibusdam fossilibus quae in montibus Uraliis inveniuntur*. Schade, Berlin. (1839) 3-5.
- [3] D. A. Egger, L. Kronik, Role of Dispersive Interactions in Determining Structural Properties of Organic–Inorganic Halide Perovskites: Insights from First-Principles Calculations, *J. Phy. Chem. Lett.*, 5 (2014) 2728-2733.
- [4] Y. Zhao, K. Zhu, Organic–inorganic hybrid lead halide perovskites for optoelectronic and electronic applications, *Chem. Soc. Rev.*, 45 (2016) 655–689.
- [5] C. Kim, T.D. Huan, S. Krishnan, R. Ramprasad, Data Descriptor: A hybrid organicinorganic perovskite dataset, *Sci. Data*, 4 (2017) 170057 (1-11).
- [6] D. Lencer, M. Salinga, M. Wuttig, Design Rules for Phase-Change Materials in Data Storage Applications, *Adv. Mater.*, 23 (2011) 2030–2058.
- [7] X. Liu, P. Long, Z. Sun, Z. Yi, Optical, Electrical and Photoelectric Properties of Layered perovskite Ferroelectric  $\text{Bi}_2\text{WO}_6$  Crystals *J. Mater. Chem. C*, 4 (2016) 7563–7570.

- [8] J.G. Bednorz, K.A. Müller, Perovskite-type oxides The new approach to high- $T_c$ , superconductivity, *Rev. Mod. Phys.*, 60 (1988) 585-600.
- [9] L. Lanzetta, J.M. Marin-Beloqui, I. Sanchez-Molina, D. Ding, S.S. Haque, Two-Dimensional Organic Tin Halide Perovskites with Tunable Visible Emission and Their Use in Light-Emitting Devices, *ACS Energy Lett.*, 2 (2017) 1662–1668.
- [10] Y. Takahashi, R. Obara, Z.Z. Lin, Y. Takahashi, T. Naito, T. Inabe, S. Ishibashi, K. Terakura, Charge-transport in tin-iodide perovskite  $\text{CH}_3\text{NH}_3\text{SnI}_3$ : origin of high Conductivity, *Dalton Trans.*, 40 (2011) 5563-5568.
- [11] A. Kojima, K. Teshima, Y. Shirai, T. Miyasaka, Organometal Halide Perovskites as Visible-Light Sensitizers for Photovoltaic Cells, *J. Am. Chem. Soc.*, 131 (2009) 6050-6051.
- [12] T.-C. Wei, S. Mokkaapati, T.-Y. Li, C.-H. Lin, G.-R. Lin, C. Jagadish, J.-H. He, Nonlinear Absorption Applications of  $\text{CH}_3\text{NH}_3\text{PbBr}_3$  Perovskite Crystals, *Adv. Funct. Mater.*, 28 (2018) 1707175 (1-8).
- [13] J. Leuthold, C. Koos, W. Freude, Nonlinear silicon photonics *Nat. Photon.*, 4 (2010) 535-544.
- [14] J.M. Hales, S. Barlow, H. Kim, S. Mukhopadhyay, J.-L. Brédas, J. W. Perry, S.R. Marder, Design of Organic Chromophores for All-Optical Signal Processing Applications, *Chem. Mater.*, 26 (2013), 549-560.
- [15] G. Lin, F. Luo, H. Pan, M.M. Smedskjaer, Y. Teng, D. Chen, J. Qiu, Q. Zhao, Universal Preparation of Novel Metal and Semiconductor Nanoparticle-Glass Composites with Excellent Nonlinear Optical Properties, *J. Phys. Chem. C*, 115 (2011) 24598-24604.
- [16] K.N. Krishnakanth, S. Seth, A. Samanta, S. Venugopal Rao, Broadband ultrafast nonlinear optical studies revealing exciting multi-photon absorption coefficients in phase pure zero-dimensional  $\text{Cs}_4\text{PbBr}_6$  perovskite films, *Nanoscale*, 11 (2019) 945-954.
- [17] S. Bouacida, H. Merazig, A. Beghidja, C. Beghidja, C. Bis(cytosinium) hexachlorostannate(IV), *Acta Crystallogr. E*, 61 (2005) m2072-m2074.
- [18] S. Bouacida, H. Merazig, A. Beghidja, C. Beghidja, Bis(adeninium) hexachlorostannate(IV)dichloride tetrahydrate, *Acta Crystallogr. E*, 61 (2005) m1153-m1155.

- [19] H.T. Li, R. Sun, H.P. Shi, S.P. Huang, 2-(2-Ammoniophenylamino)ethanaminium hexachlorostannate(IV) monohydrate, *Acta Crystallogr. E*, 61 (2005) m2088-m2089.
- [20] B.D. Ellis, C.L.B. Macdonald, Redetermination of a cyclic triphosphenium hexachlorostannate salt at 173 K, *Acta Crystallogr. E*, 62 (2006) m1235-m1236.
- [21] D.G. Billing, A. Lemmerer, M. Rademeyer, Bis(1-phenylethylammonium) hexachloridostannate(IV) and bis(2-phenylethylammonium) hexachloridostannate(IV), *Acta Crystallogr. C*, 63 (2007) m101-m104.
- [22] S. Karoui, H. Chouaib, S. Kamoun, Crystal structure, electrical transport and phase transition in 2-methoxyanilinium hexachlorido stannate(IV) dehydrate, *J. Mol. Struct.*, 1134 (2017) 180–189.
- [23] S. Karoui, S. Kamoun, Crystal Structure, Vibrational and Electrical Properties of the Bis (phenylammonium)Hexachlorotin(IV):(C<sub>6</sub>H<sub>5</sub>NH<sub>3</sub>)<sub>2</sub>\*SnCl<sub>6</sub>, *Int. J. Sci. Res. (IJSR)*, 4 (2015), 2201-2210.
- [24] X.W. Song, R.T. Xue, S.G. Chen, Y.S. Yin, Bis(4-acetylanilinium) hexachloridostannate(IV), *Acta Crystallogr. E*, 67 (2011), m653-m653.
- [25] Z. Liu, H. Dai, J. Fan, W. Yu, X. Tao, M. Jiang, Crystal structure of bis(4-methylpyridinium) hexachlorotin(IV), (C<sub>6</sub>H<sub>8</sub>N)<sub>2</sub>SnCl<sub>6</sub>, *Z. Kristallogr. NCS*, 224 (2009), 79-80.
- [26] S. Belhaj Salah, M.S. Abdelbaky, S. García-Granda, K. Essalah, C.B. Nasr, M.L. Mrad, Crystal structure, Hirshfeld surfaces computational study and physicochemical characterization of the hybrid material (C<sub>7</sub>H<sub>10</sub>N)<sub>2</sub>[SnCl<sub>6</sub>]·H<sub>2</sub>O, *J. Mol. Struct.*, 1152 (2018) 276–286.
- [27] M. Rademeyer, A. Lemmerer, D.G. Billing, Bis(4-aminopyridinium) hexachloridostannate(IV) and bis(p-toluidinium) hexachloridostannate(IV). *Acta Crystallogr. C*, 63 (2007) m289-m292.
- [28] C.J. Kane, R. Long, W.E. Pettit, G.L. Breneman, G.R. Pettit, Structure of Bis(2-chloroethyl) ammonium Hexachlorostannate, *Acta Crystallogr. C.*, 48 (1992) 1490–1491.

- [29] R.C. Gearhart, T.B. Brill, W.A. Welsh, R.H. Wood, Crystal Structure of 4-Chloropyridinium Hexachlorostannate(IV), *J. Chem. Soc., Dalton Trans.*, 4 (1973) 359-361.
- [30] M. Rademeyer, Tetrakis(anilinium) hexachlorotin(IV) dichloride, *Acta Crystallogr. E*, 60 (2004) m345–m347.
- [31] Z. Liu, H.X. Dai, D. Zhao, W.T. Yu, D.L. Cui, X.T. Tao, M.H. Jiang, Crystal structure of tetrakis(4-bromoanilinium) hexachlorotin(IV) dichloride,  $(\text{BrC}_6\text{H}_4\text{NH}_3)_4[\text{SnCl}_6]\text{Cl}_2$ , *Z. Kristallogr. NCS*, 225 (2010), 389-390.
- [32] B. Zhou, H. Liu, Tetrakis(4-chloroanilinium) hexachloridostannate(IV) dichloride, *Acta Crystallogr. E*, 68 (2012) m782-m782.
- [33] W. Xiao, R. Xue, Y. Yin, Tetrakis[(4-methoxycarbonyl)anilinium] hexachlorido stannate(IV) dichloride, *Acta Crystallogr. E*, 67 (2011) m297-m297.
- [34] C.W.M. Yuen, S.K.A. Ku, P.S.R. Choi, C.W. Kan, S.Y. Tsang, Determining Functional Groups of Commercially Available Ink-Jet Printing Reactive Dyes Using Infrared Spectroscopy, *Research Journal of Textile and Apparel*, 9 (2005) 26-38.
- [35] S. Bouacida, H. Merazig, A. Beghidja, C. Beghidja, Bis(3-carboxyanilinium) hexafluorostannate(IV), *Acta Cryst. E*, 61 (2005), m577–m579.
- [36] S.Z. Hu, Z.X. Xie, G.J. Palenik, Bond Valence Parameters for Sn(II)—X and Sn(IV)—X (X=O, S, N, C, P, As, Se, Te, F, Cl, Br, I), *Acta Phys. Chim. Sin.*, 28 (2012), 19-24.
- [37] M. O'Keeffe, N.E. Brese, Bond-Valence Parameters for Solids, *J. Am. Chem. Soc.*, 113 (1991) 3226–3229.
- [38] N.E. Brese, M. O'keeffe, Atom Sizes and Bond Lengths in Molecules and Crystals, *Acta Crystallogr. B*, 47 (1991) 192-197.
- [39] S.P. Summers, K.A. Abboud, S.R. Farrah, G.J. Palenik, Syntheses and Structures of Bismuth(III) Complexes with Nitrilotriacetic Acid, Ethylenediaminetetraacetic Acid, and Diethylenetriaminepenta acetic Acid, *Inorg. Chem.*, 33 (1994), 88-92.
- [40] I.D. Brown, *The Chemical Bond in Inorganic Chemistry*, Oxford University Press, Oxford, UK (2002).
- [41] I.D. Brown, Recent Developments in the Methods and Applications of the Bond Valence Model, *Chem. Rev.*, 109 (2009), 6858-6919.

- [42] M.A. Spackman, P.G. Byrom, A novel definition of a molecule in a crystal, *Chem. Phys. Lett.*, 267 (1997), 215–220.
- [43] M.A. Spackman, D. Jayatilaka, Hirshfeld surface analysis, *CrystEngComm*, 11 (2009) 19-32.
- [44] M.A. Spackman, J.J. McKinnon, Fingerprinting intermolecular interactions in molecular crystals, *CrystEngComm*, 4 (2002) 378-392.
- [45] L. Wang, Y.-C. Hung, S.-J. Hwu, H.-J. Koo, M.-H. Whangbo, Synthesis, Structure, and Properties of a New Family of Mixed-Framework Chalcogenide Semiconductors:  $\text{CdSbS}_2\text{X}$  (X= Cl,Br),  $\text{CdBiS}_2\text{X}$  (X= Cl,Br), and  $\text{CdBiSe}_2\text{X}$  (X=Br,I), *Chem. Mater.*, 18 (2006) 1219–1225.
- [46] C.Y. Sun, X.L. Wang, X. Zhang, C. Qin, P. Li, Z.M. Su, D.X. Zhu, G.G. Shan, K.Z. Shao, H. Wu, J. Li, Genome analysis reveals insights into physiology and longevity of the Brandt's bat *Myotis brandtii*, *Nat. Commun.*, 4 (2013), 1-8.
- [47] M. Sheik-Bahae, A.A. Said, T.H. Wei, D.J. Hagan, E.W. Van Stryland, Sensitive measurement of optical nonlinearities using a single beam, *IEEE J. Quantum Electron.* 26 (1990) 760-769.
- [48] M. Sheik-Bahae, A.A. Said, E.W. Van Stryland, High-sensitivity, single-beam  $n_2$  measurements, *Opt. Lett.*, 14(1989), 955–957.
- [49] L.W. Tutt, T.F. Boggess, A Review of Optical Limiting Mechanisms and Devices Using Organics, Fullerenes, Semiconductors and other Materials, *Progress in Quantum Electronics*, 1993, 17, 299-338.
- [50] Y. Zhou, E. Wang, J. Peng, J. Liu, C. Hu, R. Huang, X. You, Synthesis and the third-order optical nonlinearities of two novel charge transfer complexes of a heteropoly blue type  $(\text{C}_9\text{H}_7\text{NO})_4 \text{H}_7\text{PMo}_{12}\text{O}_{40} \cdot 3\text{H}_2\text{O}$  ( $\text{C}_9\text{H}_7\text{NO}$ =quinolin-8-ol) and  $(\text{phen})_3 \text{H}_7\text{PMo}_{12}\text{O}_{40} \cdot \text{CH}_3\text{CN} \cdot \text{H}_2\text{O}$  (phen=1,10-phenanthroline), *Polyhedron*, 18(10) (1999) 1419–1423.
- [51] R. W. Boyd, G. L. Fischer, in *Encyclopedia of Materials: Science and Technology* (Second Edition), <https://doi.org/10.1016/B0-08-043152-6/01107-4>, 2001, 6237-6244.
- [52] F.Z. Henari, K. Cazzini, F. El Akkari, W.J. Blau, Beam waist changes in lithium niobate during Z-scan measurement, *J. Appl. Phys.*, 78 (1995) 1373–1375.

- [53] K.M. Rahulan, A.L. Flower, N. Padmanathan, A. Mahendra, V. Shekhawat, G. Vinitha, R.A. Sujatha, M.A. Shivkumar, Luminescence and nonlinear optical properties of Er<sup>3+</sup>-doped ZnWO<sub>4</sub> nanostructures, *J. Photochem. Photobiol. A*, 386 (2020) 112128.
- [54] J.C. Johnson, Z. Li, P.F. Ndione, K. Zhu, Third-Order Nonlinear Optical Properties of Methylammonium Lead Halide Perovskite Films, *J. Mater. Chem. C*, 4 (2016) 4847-4852.
- [55] K.N. Krishnakanth, S. Seth, S. Samanta, S.V. Rao, Broadband femtosecond nonlinear optical properties of CsPbBr<sub>3</sub> perovskite nanocrystals. *Opt. lett.*, 43 (2018) 603-606.

**Table 1.**

Crystal data and structure refinement for (1) and (2)

	(1)		(2)	
Empirical formula	C <sub>24</sub> H <sub>56</sub> Cl <sub>8</sub> N <sub>4</sub> Sn		C <sub>24</sub> H <sub>56</sub> Br <sub>8</sub> N <sub>4</sub> Sn	
Formula weight g/mol	803.01		1158.67	
Temperature	296(2) K		301(2) K	
Wavelength	0.71073 Å		0.71073 Å	
Crystal system	Monoclinic		Monoclinic	
Space group	C2/m		C2/m	
Unit cell dimensions	a = 16.6981(10) Å	α = 90°	17.182(6) Å	90°
	b = 10.8131(6) Å	β = 126.97(10)°	10.993(5) Å	125.993(11)°
	c = 12.9044(8) Å	γ = 90°	13.098(4) Å	90°
Volume	1861.55(19) Å <sup>3</sup>		2001.7(13) Å <sup>3</sup>	
Z	2		2	
Density (calculated)	1.433 Mg/m <sup>3</sup>		1.922 Mg/m <sup>3</sup>	
Absorption coefficient	1.281 mm <sup>-1</sup>		8.642 mm <sup>-1</sup>	
F(000)	828		1116	
Crystal size	0.150 x 0.150 x 0.100 mm <sup>3</sup>		0.230 x 0.280 x 0.310 mm <sup>3</sup>	
Theta range for data collection	3.054 to 30.536°		3.55 to 30.04°	
Index ranges	-20 ≤ h ≤ 23, -15 ≤ k ≤ 15, -18 ≤ l ≤ 18		-24 ≤ h ≤ 24, -12 ≤ k ≤ 15, -18 ≤ l ≤ 15	
Reflections collected	20224		8091	
Independent reflections	2937 [R(int) = 0.0544]		2994 [R(int) = 0.0600]	
Data / restraints / parameters	2937 / 204 / 161		2994 / 0 / 92	
Goodness-of-fit on F <sup>2</sup>	1.292		1.067	

Absorption correction	Semi-empirical from equivalents	Semi-empirical from equivalents
Max. and min. transmission	0.7461 and 0.5791	0.7460 and 0.2994
Refinement method	Full-matrix least-squares on F <sup>2</sup>	Full-matrix least-squares on F <sup>2</sup>
Final R indices [I > 2σ(I)]	R1 = 0.0511, wR2 = 0.1135	R1 = 0.0537, wR2 = 0.1489
R indices (all data)	R1 = 0.0670, wR2 = 0.1321	R1 = 0.0757, wR2 = 0.1613
Extinction coefficient	n/a	n/a
Largest diff. peak and hole	1.065 and -1.195 e.Å <sup>-3</sup>	1.110 and -1.593 e.Å <sup>-3</sup>
<b>CCDC</b>	<b>1992840</b>	<b>1992842</b>

**Table 2.**parameters for compounds **(1)** and **(2)**

	<b>(1)</b>		<b>(2)</b>
	<b>Bond distances</b>		<b>Bond distances</b>
Sn1-Cl1	2.4192(9) Å	Sn1-Br1	2.5868(9) Å
Sn1-Cl1 <sup>i</sup>	2.4192(9) Å	Sn1-Br1 <sup>i</sup>	2.5868(9) Å
Sn1-Cl2	2.4561(3) Å	Sn1-Br2	2.6288(13) Å
Sn1-Cl2 <sup>i</sup>	2.4561(3) Å	Sn1-Br1 <sup>ii</sup>	2.5868(9) Å
Sn1-Cl1 <sup>ii</sup>	2.4192(9) Å	Sn1-Br2 <sup>i</sup>	2.6288(13) Å
Sn1-Cl1 <sup>iii</sup>	2.4192(9) Å	Sn1-Br1 <sup>iii</sup>	2.5868(9) Å
Average bond length (Å)	<b>2.4315</b>		<b>2.6008</b>
Polyhedral volume (Å <sup>3</sup> )	<b>19.1617</b>		<b>23.4499</b>
Distortion index (bond length)	<b>0.00674</b>		<b>0.00718</b>
Quadratic elongation	<b>1.0003</b>		<b>1.0002</b>
Bond angle variance (deg. <sup>2</sup> )	<b>0.5377</b>		<b>0.3827</b>
Effective coordination number	<b>5.9896</b>		<b>5.9882</b>

**Table 3a.** Hydrogen bonds for (1) [ $\text{\AA}$  and  $^\circ$ ]

D-H...A	d(D-H)	d(H...A)	d(D...A)	$\angle(\text{DHA})$
C(4A <sup>a</sup> )-H(4A1 <sup>a</sup> )...Cl(1)	0.97	2.92	3.861(16)	164.3
N(2A <sup>a</sup> )-H(2A1 <sup>a</sup> )...Cl(3)	0.89	2.29	3.098(9)	150.1
N(2A <sup>a</sup> )-H(2A2 <sup>a</sup> )...Cl(3)#3	0.89	2.28	3.170(11)	176
N(1A <sup>c</sup> )-H(1A3 <sup>c</sup> )...Cl(3)	0.89	2.23	3.11(3)	173.7
N(1A <sup>c</sup> )-H(1A4 <sup>c</sup> )...Cl(1)	0.89	2.77	3.432(19)	132.1
N(1A <sup>c</sup> )-H(1A4 <sup>c</sup> )...Cl(1)#1	0.89	2.77	3.432(19)	132.1
N(1A <sup>c</sup> )-H(1A4 <sup>c</sup> )...Cl(2)#2	0.89	2.66	3.364(3)	136.9

Symmetry transformations used to generate equivalent atoms:

#1  $x, -y+1, z$  #2  $-x+1, -y+1, -z$  #3  $-x, -y+1, -z-1$

**Table 3b.**

Hydrogen bonds for (2) [ $\text{\AA}$  and  $^\circ$ ]

D-H...A	d(D-H)	d(H...A)	d(D...A)	$\angle(\text{DHA})$
C(4)-H(6B <sup>a</sup> )...Br(1)	0.97	3.02	3.901	151.9
C(4)-H(6B <sup>b</sup> )...Br(1)	0.97	3.02	3.901	151.9
N(2)-H(2B <sup>a</sup> )...Br(3)	0.89	2.58	3.250	132.5
N(1)-H(1A <sup>a</sup> )...Br(3)	0.89	2.36	3.250	177.1
N(1)-H(1B <sup>a</sup> )...Br(1)	0.89	2.96	3.569	127.3
N(1)-H(1B <sup>b</sup> )...Br(2)	0.89	2.77	3.525	143.0
N(1)-H(1B <sup>c</sup> )...Br(1)	0.89	2.96	3.569	127.3

Symmetry transformations used to generate equivalent atoms:

**Table 4.**

Bond valence sum calculation of compounds (1) and (2)

Compound	Co. No.	Bond distances (Å)						V = $\sum v_{ij}$
		Sn1-Cl1	Sn1-Cl1 <sup>i</sup>	Sn1-Cl1 <sup>ii</sup>	Sn1-Cl1 <sup>iii</sup>	Sn1-Cl2	Sn1-Cl2 <sup>i</sup>	
(1)	6	2.4192(9)	2.4192(9)	2.4192(9)	2.4192(9)	2.4561(13)	2.4561(13)	3.95*
		Sn1-Br1	Sn1-Br1 <sup>i</sup>	Sn1-Br2	Sn1-Br1 <sup>ii</sup>	Sn1-Br1 <sup>iii</sup>	Sn1-Br2 <sup>i</sup>	
(2)	6	2.5868(8)	2.5868(8)	2.6288(9)	2.5868(8)	2.5868(8)	2.6288(9)	3.93*

\* Values rounded off

**Table 5.**

Third-order NLO parameters of (1) and (2)

Third-order NLO Parameters	Calculated values	
	(1)	(2)
Nonlinear refractive index ( $n_2$ ) (cm <sup>2</sup> /W)	$6.17 \times 10^{-10}$	$2.35 \times 10^{-9}$
Nonlinear absorption coefficient ( $\beta$ ) (cm/W)	$2.82 \times 10^{-5}$	$9.70 \times 10^{-5}$
Real part of the third-order susceptibility [ $\text{Re}(\chi^3)$ ] (esu)	$2.11 \times 10^{-7}$	$1.91 \times 10^{-6}$
Imaginary part of the third-order susceptibility [ $\text{Im}(\chi^3)$ ] (esu)	$4.37 \times 10^{-7}$	$2.08 \times 10^{-7}$

Third-order nonlinear optical susceptibility ( $\chi^{(3)}$ ) (esu)  $4.85 \times 10^{-7}$   $1.92 \times 10^{-6}$

**Table 6.**

Comparison of third-order nonlinear susceptibility ( $\chi^{(3)}$ ) of some perovskite materials

Specimen	$\chi^{(3)}$ (esu)	Ref
LiNbO <sub>3</sub>	$1.7 \times 10^{-5}$	[52]
ZnWO <sub>4</sub>	$2.32 \times 10^{-6}$	[53]
CH <sub>3</sub> NH <sub>3</sub> PbBr <sub>3</sub>	$1.6 \times 10^{-6}$	[54]
CsPbBr <sub>3</sub> nanocubes	$4.3 \times 10^{-10}$	[55]
CsPbBr <sub>3</sub> nanorods	$9.5 \times 10^{-10}$	[55]
(1)	$4.85 \times 10^{-7}$	Present work
(2)	$1.92 \times 10^{-6}$	Present work

**Table 7.**

Mass losses in compounds (1) and (2)

	Mass loss (%)	Decomp. range (°C)	Fragment lost
	67.3 (calcd.: 67.6)	240 –397	4(C <sub>6</sub> H <sub>14</sub> NCl)
C <sub>24</sub> H <sub>56</sub> Cl <sub>8</sub> N <sub>4</sub> Sn (1)	17.6 (calcd.: 17.7)	398-498	4Cl
	14.8 (calcd.: 14.8)	> 499	Residual Sn

	61.9 (calcd.: 62.2)	245 –402	evaporation
$C_{24}H_{56}Br_8N_4Sn$ (2)	27.5 (calcd.: 27.6)	403–513	$4(C_6H_{14}NBr)$
	10.2 (calcd.: 10.2)	> 514	Residual Sn evaporation

---

### Figure Captions

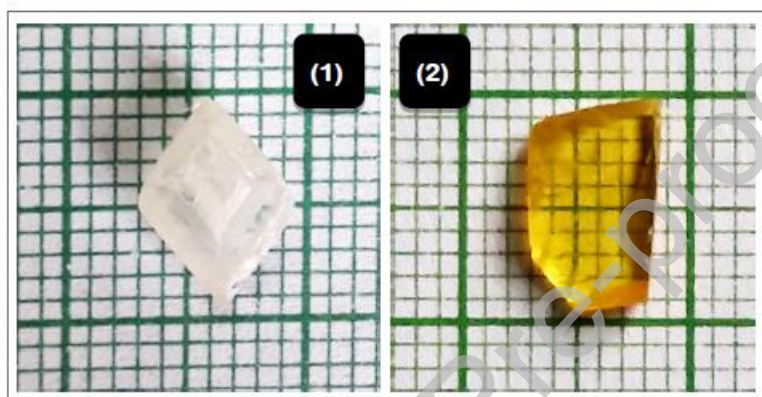


**Fig. 1.** Photographs of as-grown crystals (1) and (2)

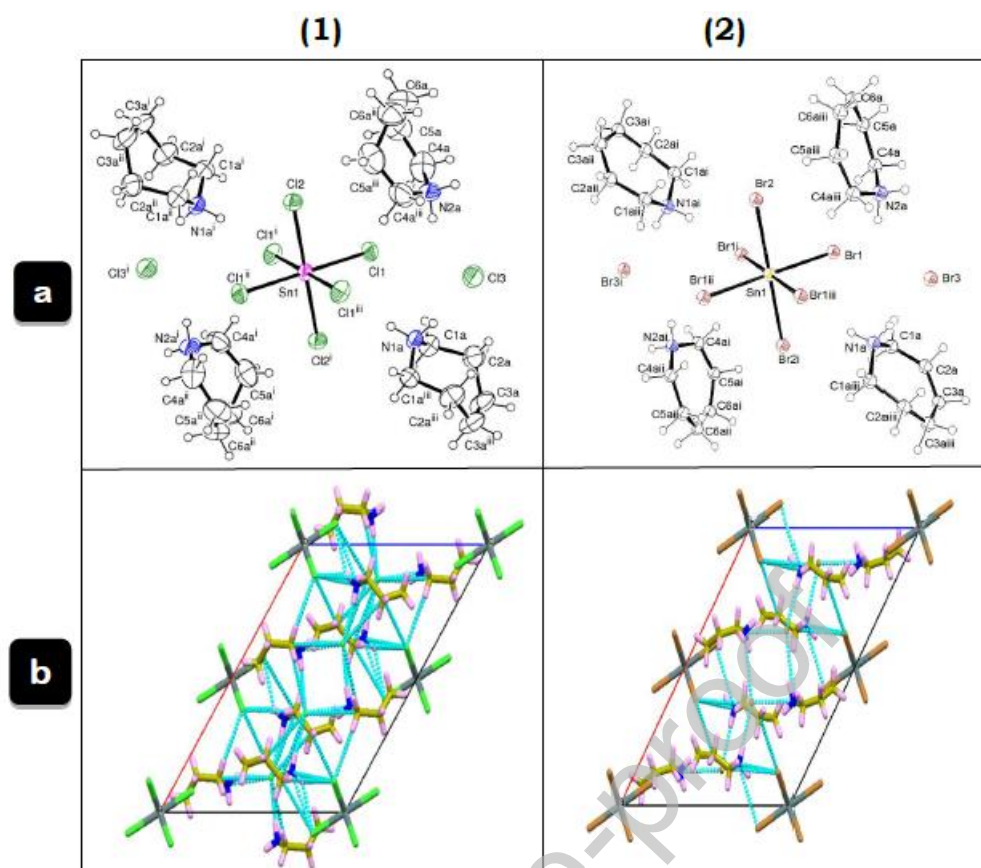


**Fig. 2.** (a) ORTEP and (b) packing diagram of (1) and (2) (hydrogen bonds as blue dashed lines)

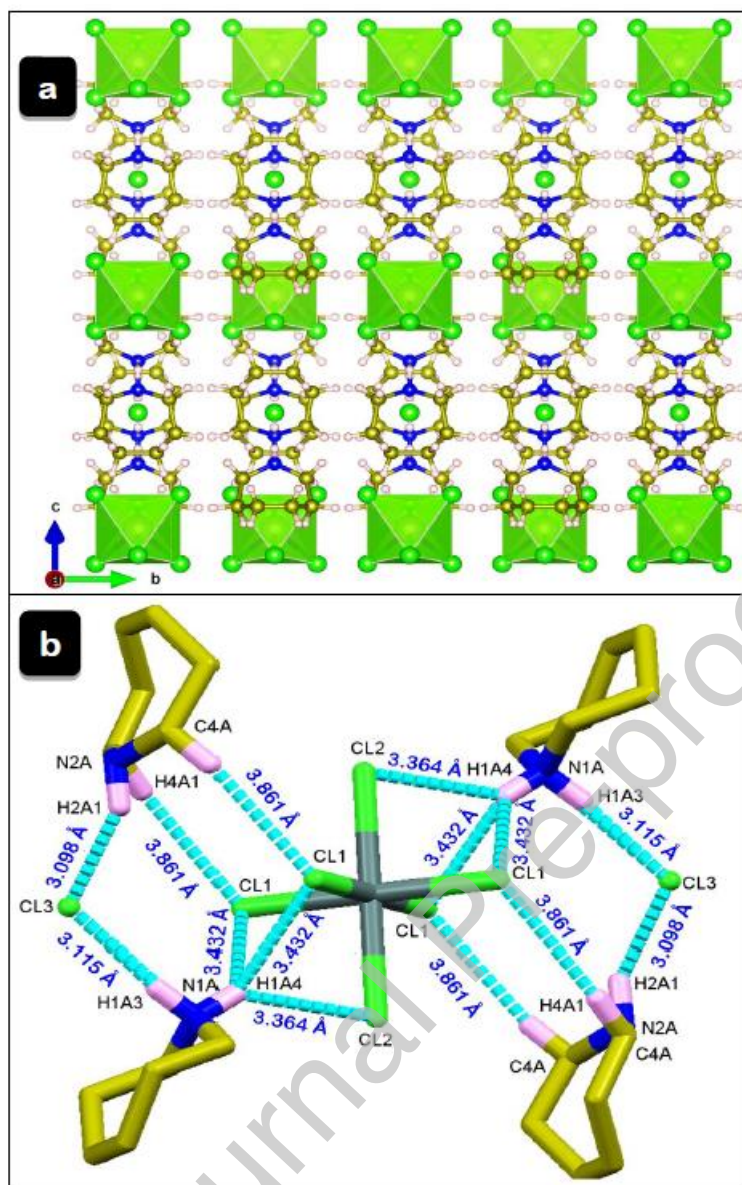


**Fig. 3.** (a) Diagram of the layered packing and octahedra viewed along the a-axis and (b) hydrogen-bonding network for compound (1) (most of the hydrogens are omitted for clarity)

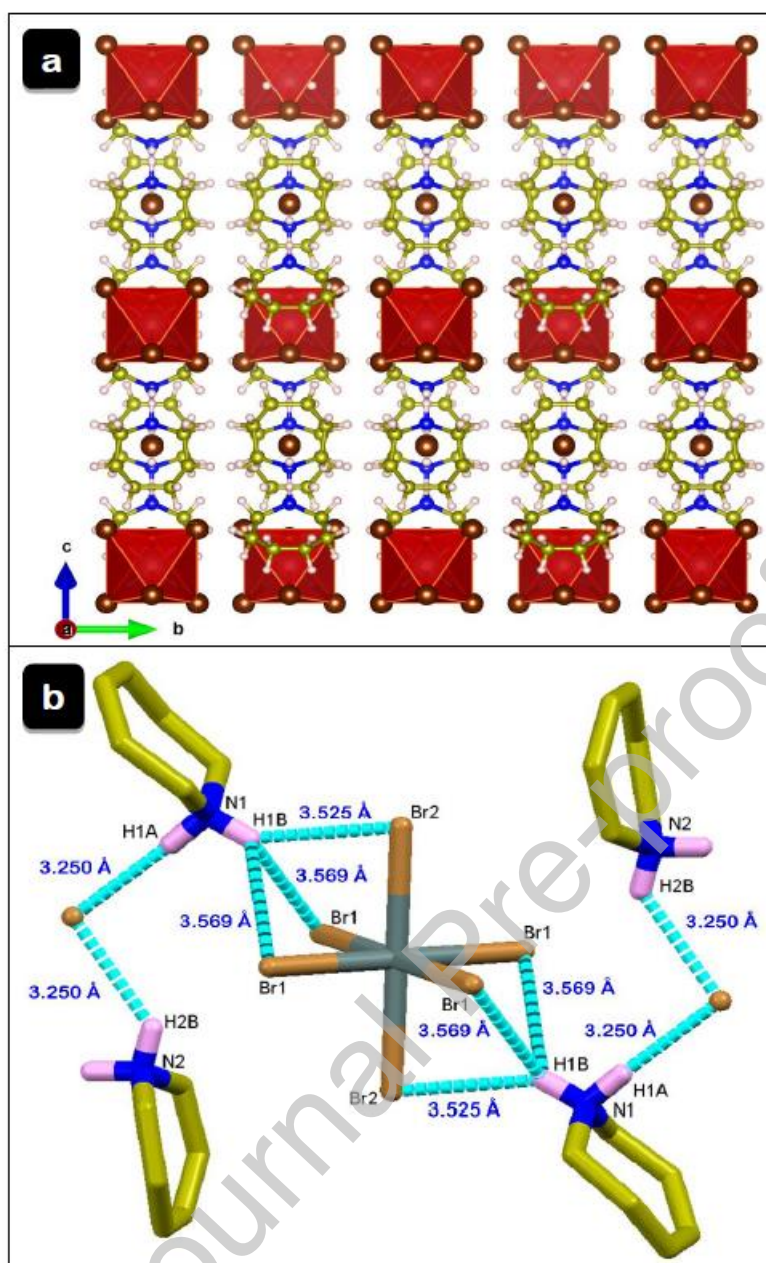


**Fig. 4.** (a) Diagram of the layered packing and octahedra viewed along the a-axis and (b) hydrogen-bonding network for compound (2) (most of the hydrogens are omitted for clarity)

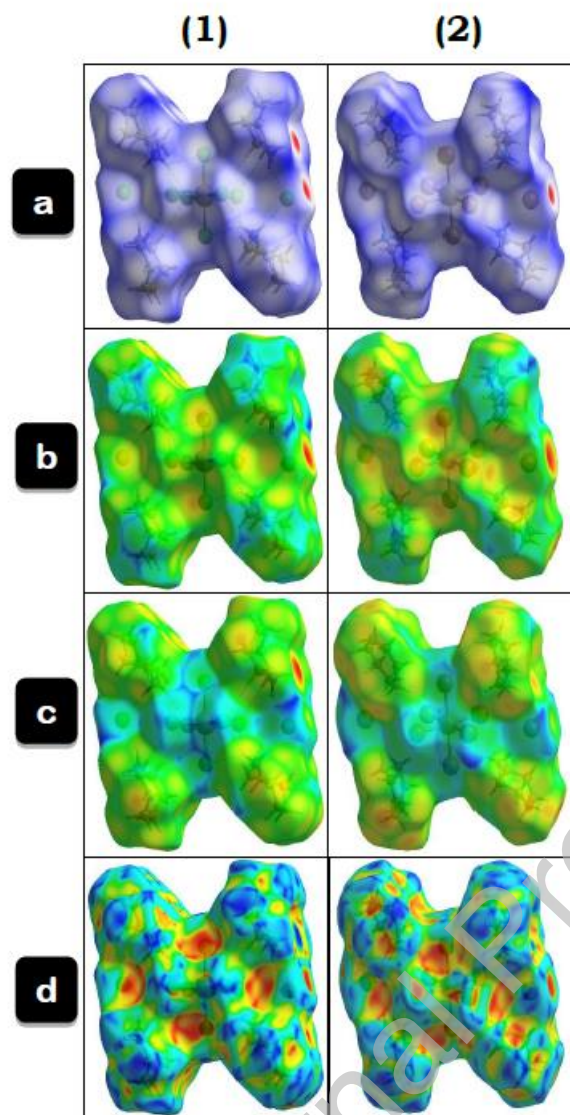


**Fig. 5.** Hirshfeld surface analysis of (1) and (2) (a)  $d_{\text{norm}}$  (b)  $d_e$  (c)  $d_i$  and (d) shape index

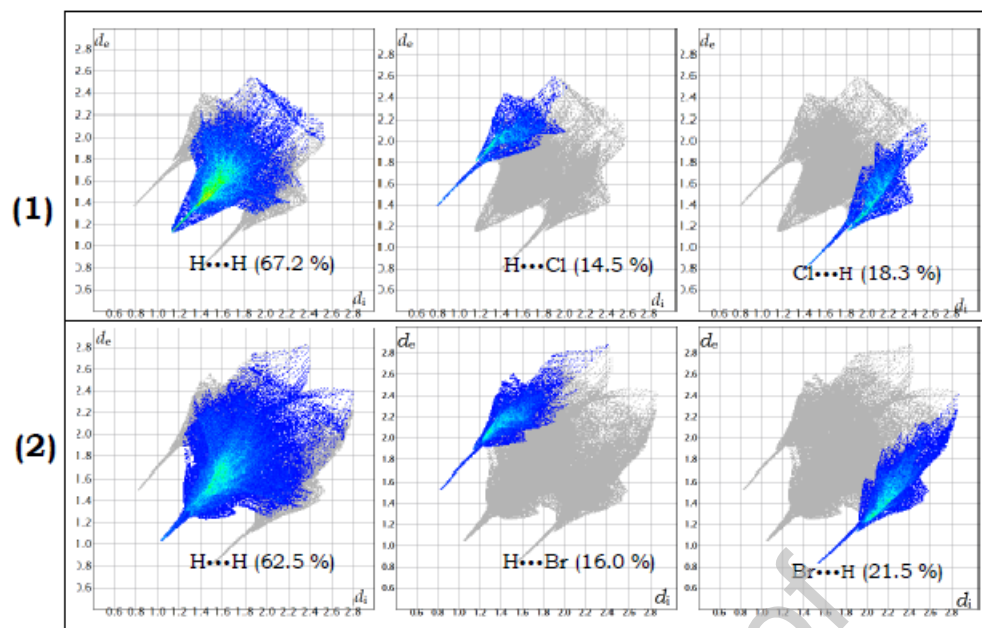


Fig. 6. Fingerprint plots of (1) and (2)

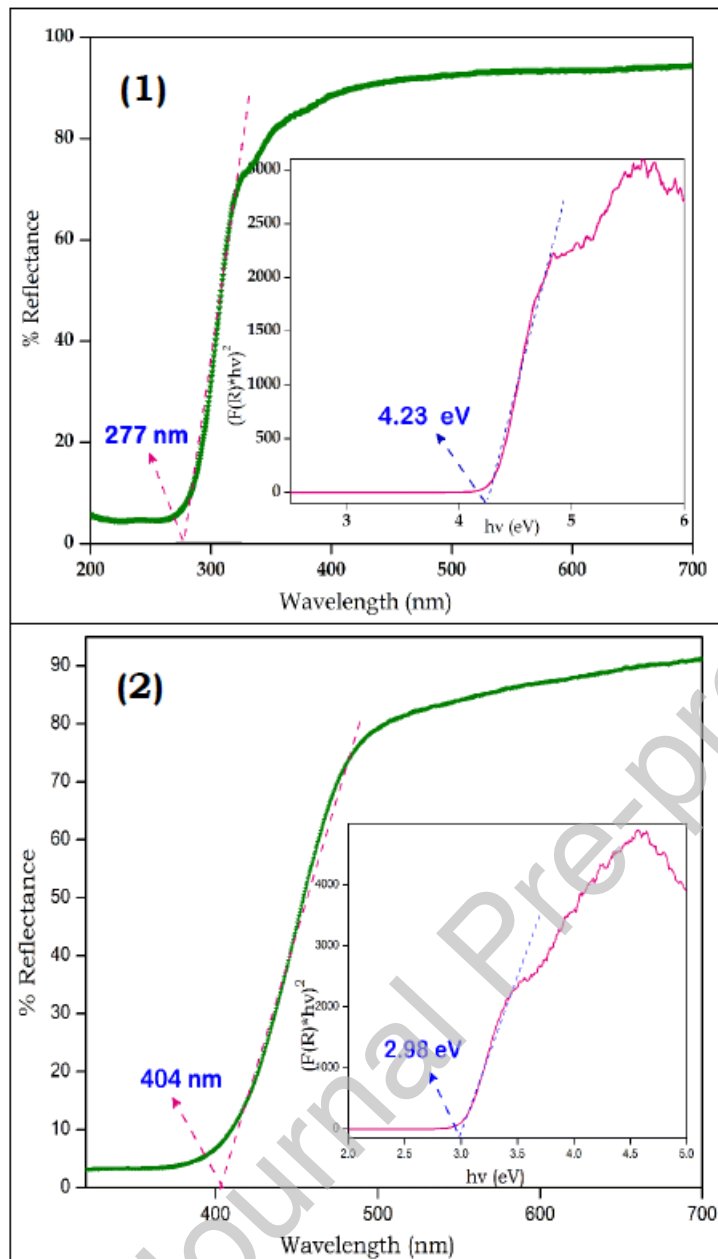
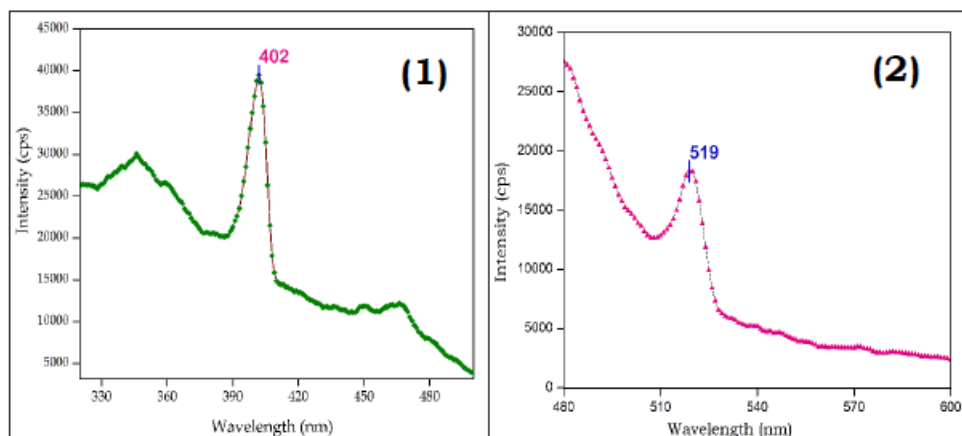
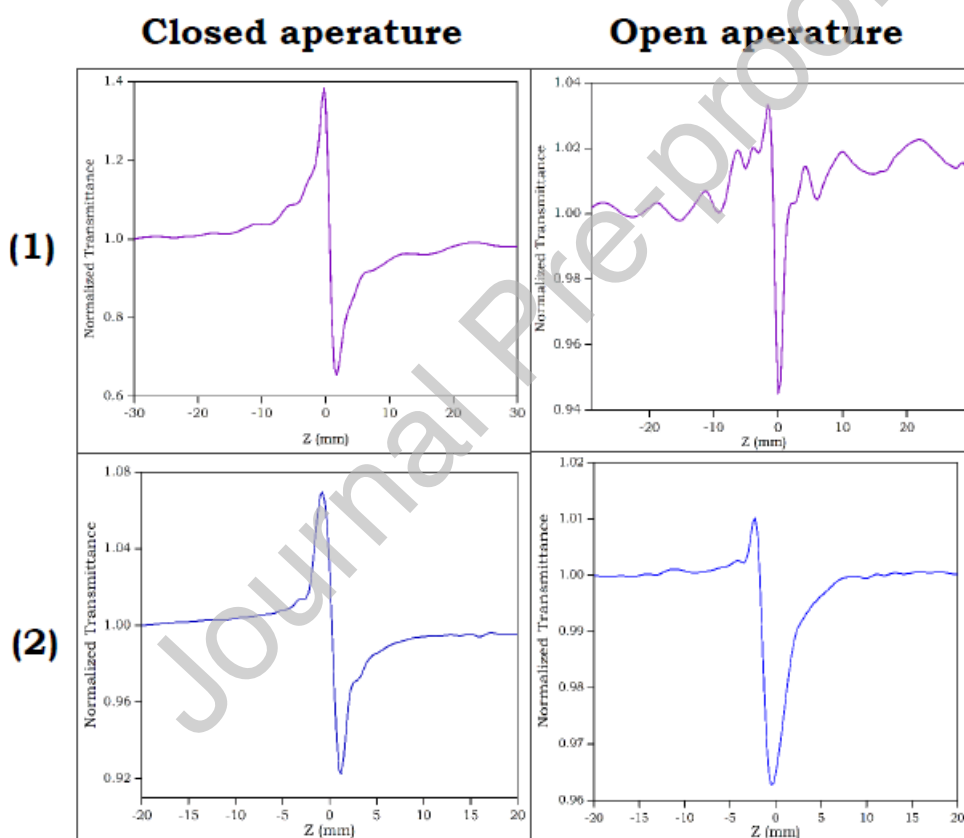


Fig. 7. UV spectra (Tauc plot is given as an inset) of (1) and (2)



**Fig. 8.** PL spectra of compounds (1) and (2) solid-state at room temperature



**Fig. 9.** Closed and open aperture Z-scan curves of (1) and (2)

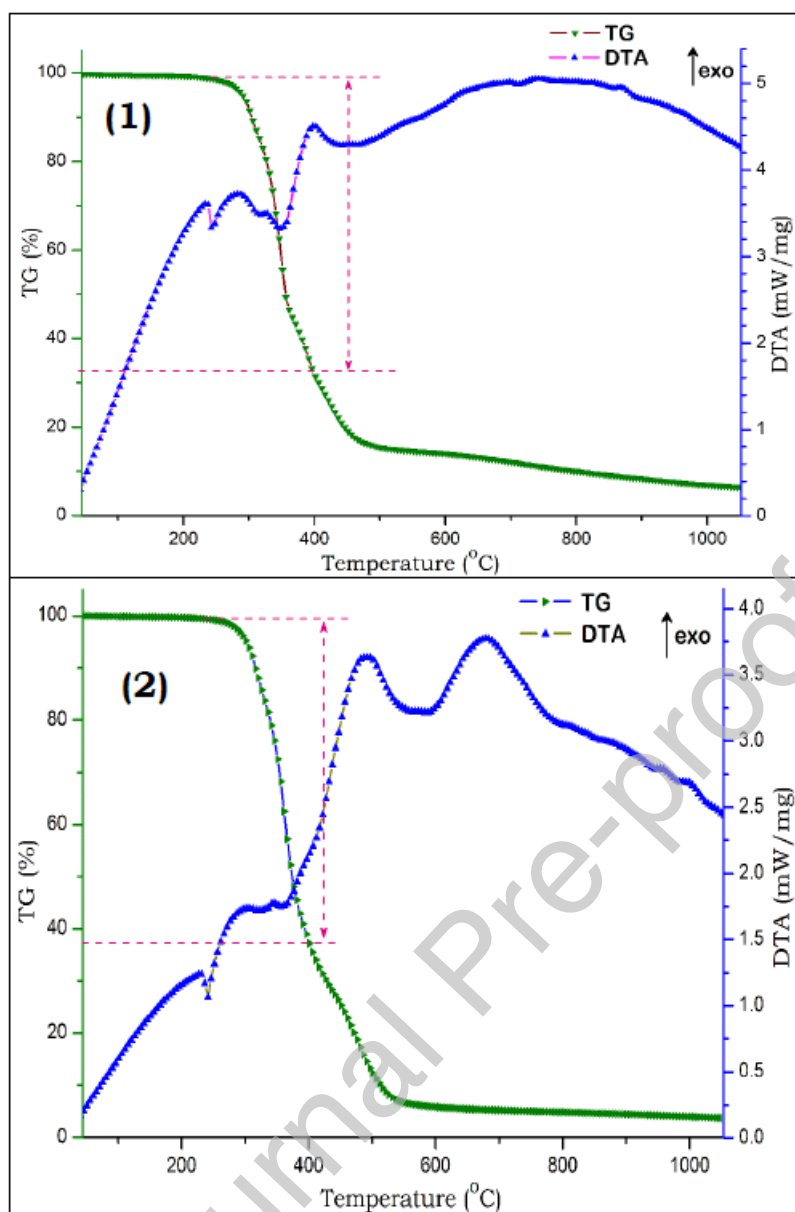
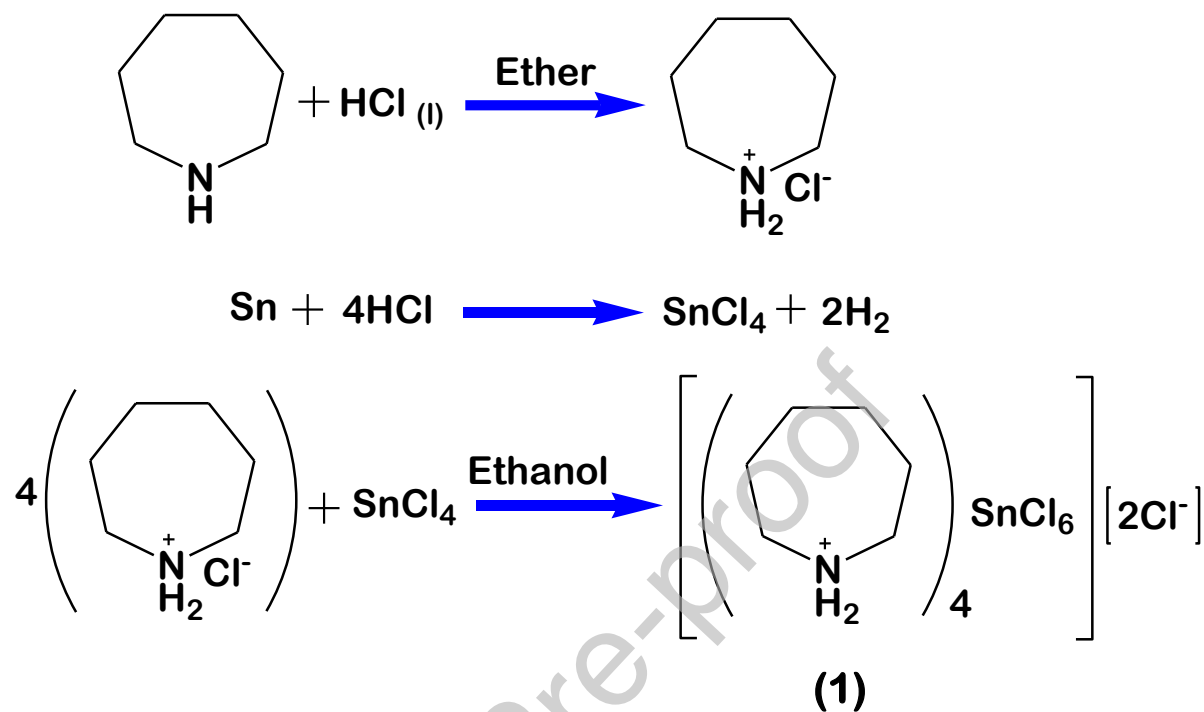


Fig. 10. TG-DTA curves of (a) (1) and (b) (2)

**Scheme**

Preparation of tetrakis(azepanium) hexachlorostannate(IV) dichloride (1)



**Scheme 1.** Preparation of compound (1)

Preparation of tetrakis(azepanium) hexabromostannate(IV) dibromide (2)

